J Mater Sci: Mater Electron **(2025) 36:218**

Fabrication and thermoelectric properties of nano Sb_2Te_3, Bi_2Te_3 thin films using PVD of synthesized nano powder

Mahmoud Rezaee Roknabadi[1], Masoud Mollaee[1,*], and Somayyeh Garazhian[1]

[1] *Department of Physics, Faculty of Science, Ferdowsi University of Mashhad, Mashhad, Iran*

Received: 30 November 2024
Accepted: 17 January 2025

ABSTRACT

This study explores the fabrication and thermoelectric properties of Sb_2Te_3 and Bi_2Te_3 thin films prepared using physical vapor deposition (PVD) with synthesized nano powders as source materials. Nano Sb_2Te_3 and Bi_2Te_3 powders were synthesized via a hydrothermal method, yielding high-purity nanostructures with hexagonal crystal structures, as confirmed by X-ray diffraction (XRD). The nano powders were deposited onto substrates to create thin films approximately 100 nm thick, with scanning electron microscopy (SEM) confirming uniform morphology. Thermoelectric characterization revealed a Seebeck coefficient of 192 μV/K for Sb_2Te_3 at room temperature, which increased to 380 μV/K after annealing. Bi_2Te_3 exhibited an n-type Seebeck coefficient of − 45 μV/K, which improved to − 170 μV/K with annealing. Resistivity measurements demonstrated distinct electrical transport mechanisms for both materials, with Sb_2Te_3 exhibiting metallic-like behavior at lower temperatures and Bi_2Te_3 showing thermally activated conduction. The complementary thermoelectric properties of Sb_2Te_3 and Bi_2Te_3 highlight their potential for use in high-efficiency p–n junction thermoelectric devices.

1 Introduction

Thermoelectric materials have garnered significant interest for their ability to directly convert thermal energy into electrical energy, offering promising applications in sustainable energy generation. These materials are particularly valuable for waste heat recovery, powering small-scale electronics, and contributing to green energy solutions, as they reduce reliance on traditional fossil fuels [1–5]. Among thermoelectric materials, bismuth telluride (Bi_2Te_3) and antimony telluride (Sb_2Te_3) stand out due to their high thermoelectric efficiency within intermediate temperature ranges, where they exhibit desirable properties such as excellent electrical conductivity, low thermal conductivity, and a substantial Seebeck coefficient—traits critical to efficient thermoelectric performance [6–11].

In recent years, the nano structuring of thermoelectric materials has been shown to significantly improve their performance by enhancing the thermoelectric figure of merit (ZT) through phonon scattering and reduced lattice thermal conductivity [12–14]. This has led to the exploration of nano-scale thin-film forms of Bi_2Te_3 and Sb_2Te_3, where quantum confinement effects

---

Address correspondence to E-mail: m.mollaee@um.ac.ir

https://doi.org/10.1007/s10854-025-14313-0

contribute to improved charge carrier transport properties [11, 15]. Various deposition techniques, including molecular beam epitaxy (MBE), chemical vapor deposition (CVD), and physical vapor deposition (PVD), have been employed to fabricate these nanostructured films [2, 16]. Each technique presents distinct advantages; for instance, MBE offers high crystallinity [17], while CVD allows for large-area deposition. PVD, in particular, is advantageous due to its relatively simple setup, precise thickness control, and ability to yield high-purity thin films.

Previous studies have investigated the thermoelectric properties of Bi_2Te_3 and Sb_2Te_3 PVD derived thin films [6, 18, 19]. For example, Hong et al. demonstrated the 500 nm-thick Sb_2Te_3 films deposited onto SiO2/Si substrates with Seebeck coefficient of 283 µV/K after annealing at room temperature [6]. Similarly, Wanarattikan et al. reported that PVD-derived Sb_2Te_3 films exhibited improved thermoelectric properties when synthesized with optimized nano powders, showing a substantial reduction in thermal conductivity due to grain boundary scattering [8]. Kim et al. showed the effect of annealing on the thermoelectric properties of both Bi_2Te_3 and Sb_2Te_3 thin films [20]. They found a power factor of 1600 $\mu W/K^2 \cdot m$ for Sb_2Te_3 and around 700 $\mu W/K^2 \cdot m$ for Bi_2Te_3. similar strategy of using nanostructure composites was highlighted by Kumar et al. [21], where Sb_2Te_3/ZnTe nanostructure composites achieved a notable improvement in thermoelectric properties. For $Zn_{0.5}Sb_{1.5}Te_3$ composites, the Seebeck coefficient and electrical conductivity increased simultaneously due to the variable range hopping transport mechanism, achieving a power factor of 33 $\mu W/mK^2$ at 425 K. In another study polyaniline-Bi–Sb–Te–Se thin films were fabricated by electrodeposition and electrochemical reaction method and the highest obtained seebeck coefficient was about 30 µV/K [22]. In 2023, Thaowonkaew et al. [23] fabricated Ag-doped SbTe thin film by RF magnetron sputtering technique and the maximum obtained power factor was 4600 $\mu W/mK^2$. Recently, Cheng et al. [24] used PECVD technique to study the effect of diffusion on thermoelectric properties of Bi_2Te_3. They found Cu atoms diffuse into the Bi_2Te_3 film, forming $Cu_{2-x}Te$ intermetallic compounds on the surface, while Ni atoms penetrate approximately 50 nm into the Bi_2Te_3 layer. Long-term aging leads to a decrease in the power factor of Ni/Bi_2Te_3/Ni samples, attributed to the conversion of n-type Bi_2Te_3 to p-type due to the formation of Bi–Te antisite defects. In contrast, Cu diffusion in Cu/Bi_2Te_3/Cu samples significantly mitigates the PF degradation during extended aging. The maximum power factor obtained was about 370 $\mu W/mK^2$.

Group IV materials, such as SiGe and GeSn, have also been extensively studied for thermoelectric applications [25, 26]. However, these materials often exhibit higher thermal conductivity and limited efficiency at low temperatures. For instance, SiGe nanowires achieve power factors exceeding 2000 $\mu W/mK^2$ at elevated temperatures (> 400 K) but lack efficiency in intermediate temperature ranges. Moreover, thin films offer several advantages over nanowires, including easier integration into devices, greater mechanical robustness, and enhanced control over material properties, making them more practical for scalable applications.

This study investigates the fabrication and thermoelectric properties of Sb_2Te_3 and Bi_2Te_3 thin films prepared via PVD using synthesized nano powders. The nano powders, synthesized through a hydrothermal method, enabled the deposition of uniform, high-purity thin films, as confirmed by SEM analysis. Thermoelectric characterization revealed a significant improvement in the Seebeck coefficient and power factor for Sb_2Te_3 thin films, reaching 380 µV/K after annealing, while Bi_2Te_3 exhibited complementary n-type behavior with -170 µV/K seebeck coefficient after annealing. The results highlight the role of nano structuring, annealing, and precise deposition techniques in achieving high-performance thermoelectric materials. This research provides a scalable and cost-effective pathway for developing advanced thermoelectric materials suitable for energy harvesting and thermal management applications.

2 Experimental method

The synthesis of Sb_2Te_3 and Bi_2Te_3 nano powders was conducted using a hydrothermal method designed to achieve high purity and controlled particle size. For the preparation of Sb_2Te_3, a solution of 0.55 mmol ethylenediaminetetraacetic acid (EDTA) was first dissolved in 5 mL of distilled water under continuous magnetic stirring. Subsequently, 40 mL of ethanol was added, and the solution was stirred for 10 min to ensure homogeneity. After this, 5 mmol of $SbCl_3$ was introduced and allowed to dissolve completely, followed by the addition of 7.5 mmol of Te powder and 10 mmol of $NaBH_4$. The resulting mixture was stirred for an additional 20 min and then transferred into a nitrogen-filled glove box to maintain an inert environment. The reaction proceeded at 200 °C for 24 h, after which it was allowed to cool to room temperature. The resulting black precipitates were collected, filtered, and washed with distilled water, ethanol, and acetone to remove any impurities, then air-dried under a nitrogen atmosphere to prevent oxidation.

The synthesis of Bi_2Te_3 followed a similar protocol, with $BiCl_3$ replacing $SbCl_3$ as the starting reagent. Using the same reaction conditions ensured consistency in the particle size and purity of both materials. $BiCl_3$ was dissolved along with Te powder and $NaBH_4$ in the same inert, high-temperature environment. This consistent synthesis approach allowed for uniformity in the properties of the resulting nano powders, facilitating a controlled comparison of thermoelectric performance in subsequent experiments.

The prepared Sb_2Te_3 and Bi_2Te_3 nano powders were then utilized as source materials for thin film deposition via physical vapor deposition (PVD). The deposition was carried out in a high-vacuum chamber with a base pressure of 2×10^{-6} Torr, using tungsten boats to heat the nano powders to evaporation. A clean glass substrate was selected and heated to 150 °C, enhancing the adhesion and quality of the resulting films. For the deposition of Sb_2Te_3, the nano powder was first subjected to a 12-h vacuum environment at a working pressure of 6×10^{-5} Torr to ensure uniform evaporation. The evaporation rate was carefully maintained at 20 Å/s, achieving a target film thickness of approximately 100 nm. The Bi_2Te_3 deposition followed the same conditions as Sb_2Te_3, with similar thickness and surface morphology control, ensuring comparable films for analysis.

Once the deposition was complete, the thermoelectric properties of the Sb_2Te_3 and Bi_2Te_3 thin films were characterized. Measurements of the Seebeck coefficient, electrical conductivity, and specific resistivity were performed to assess the thermoelectric performance. Structural and surface morphology analyses, including X-ray diffraction (XRD) and scanning electron microscopy (SEM), confirmed the composition, crystallinity, and homogeneity of the films. These analyses provided insights into the quality of the films and their potential for thermoelectric applications, aligning with the study's objective of exploring effective fabrication methods for high-performance thermoelectric materials.

3 Results and discussion

The X-ray Diffraction (XRD) analysis of the Sb_2Te_3 nano powder confirmed a hexagonal structure, with prominent diffraction peaks observed at 28°, 39°, and 52°, indexed to the (015), (1010), and (205) planes as shown in Fig. 1a. These align well with the reported crystallographic data for Sb_2Te_3, confirming the synthesized material's phase purity and crystal integrity. The lattice parameters $a = 30.451$ Å and $c = 4.262$ Å are consistent with established literature values, and

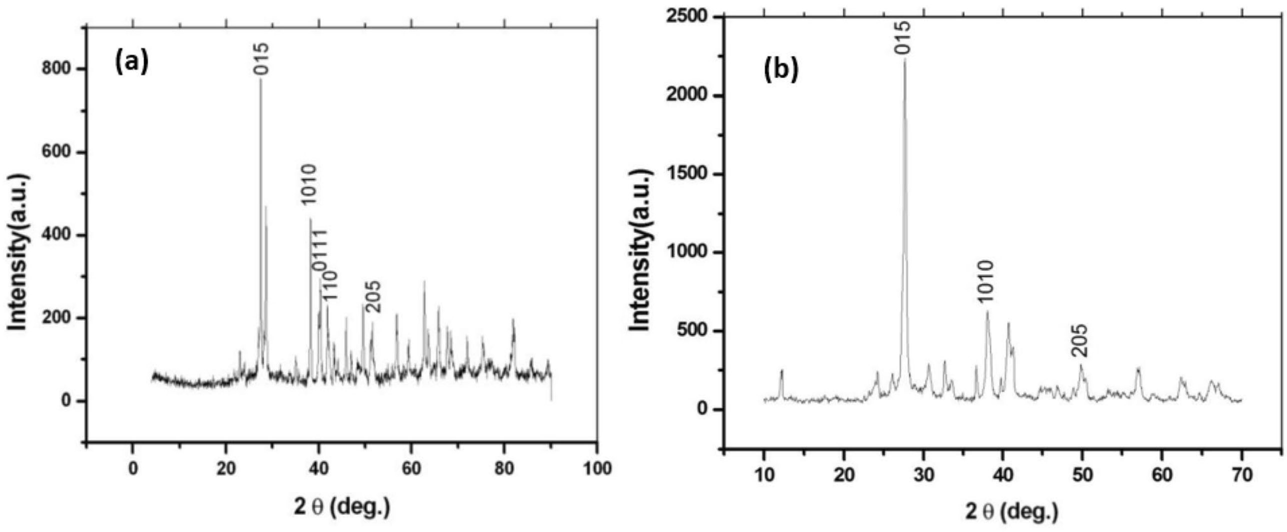

Fig. 1 XRD diagram of **a** Sb_2Te_3 nano powder, **b** Bi_2Te_3 nano powder

the average grain size, calculated to be around 50 nm using the Scherrer equation (Eq. 1), is in the desired nano-range. The X-ray diffraction pattern related to Bi_2Te_3 nanoparticles in the range of $10 < 2\theta < 70$, is shown in Fig. 1b. According to the diffraction pattern, the hexagonal crystal structure of the Bi_2Te_3 phase with parameters $a = b = 4.385$ Å and $c = 30.483$ Å and space group $R\bar{3}m$ is observed, as indicated in the figure. The reference peaks corresponding to the planes [015], [110], and [201] with 2θ values of 27.55, 37.92, and 45.10, respectively, indicate the presence of the Bi_2Te_3 phase in the material [27].

$$D = \frac{K\lambda}{\beta cos\theta} \tag{1}$$

The crystallite size (D) is calculated using the Scherrer equation, where D represents the size of crystalline domains, measured in nanometers (nm). The shape factor (K) is a dimensionless constant, often set to 0.89 or 1, depending on the assumed shape of the crystallites which here assumed to be a unity. The X-ray wavelength ($\lambda = 0.15$ nm) is a known constant. The full width at half maximum (β) is the peak broadening measured in radian. Finally, the Bragg angle (θ) is the diffraction angle corresponding to the peak.

To find average gain size the Eq. 2 was used:

$$\langle D\rangle_{\text{weighted}} = \frac{\sum(D_i \cdot I_i)}{\sum I_i}. \tag{2}$$

Which I_i is relative intensity. With the standard deviation of Eq. 3:

$$\sigma_D = \sqrt{\frac{\sum(D_i - \langle D\rangle)^2}{N}} \tag{3}$$

This nano-scale grain size is crucial because it directly impacts the material's ability to enhance phonon scattering at grain boundaries, significantly reducing the lattice component of thermal conductivity. Phonons, which are the primary carriers of thermal energy in solids, encounter increased resistance at the numerous grain boundaries introduced by the nano-sized grains. This scattering mechanism disrupts the heat flow, effectively lowering thermal conductivity while maintaining favorable electronic transport properties, which is critical for optimizing the thermoelectric properties [28]. The reduction in thermal conductivity without adversely affecting electrical conductivity or the Seebeck coefficient is a key advantage of nano-scale engineering, enabling improved thermoelectric efficiency. Numerous studies have reported that reducing grain size to the nano-scale enhances thermoelectric performance in materials due to enhanced phonon scattering [29, 30]. Tables 1 and Table 2 show crystallite size of Sb_2Te_3 and Bi_2Te_3 calculated using the Scherrer equation for different XRD peaks, respectively. So the crystalline size for Sb_2Te_3 is $\langle D\rangle = 50.53\,\text{nm} \pm 8.99\,\text{nm}$, and for Bi_2Te_3 is $\langle D\rangle = 33.75\,\text{nm} \pm 5.93\,\text{nm}$.

Table 1 Crystallite size of Sb_2Te_3 calculated using the Scherrer equation for different XRD peaks

hkl	Cos(θ)	β	Intensity (cps)	Grain size (nm)
015	0.97	0.0034	100	45.48
1010	0.94	0.0034	55	46.9
0111	0.94	0.0034	30	46.9
110	0.93	0.0021	25	76.8
205	0.90	0.0027	14	61.7

Table 2 Crystallite size of Bi_2Te_3 calculated using the Scherrer equation for different XRD peaks

hkl	Cos(θ)	β	Intensity (cps)	Grain size (nm)
015	0.97	0.0048	100	32.22
1010	0.95	0.0048	57	32.89
110	0.94	0.0034	35	46.93
205	0.91	0.0082	19	20.10

Following physical vapor deposition (PVD), SEM imaging of the Sb_2Te_3, Bi_2Te_3 thin films revealed a highly uniform surface with grain sizes in the 50–100 nm range as shown in Fig. 2. This homogeneity in morphology can be attributed to using nano-structured Sb_2Te_3, Bi_2Te_3 powder as the precursor, which promotes consistent, fine-grained deposition. This uniformity across the film's surface is advantageous for optimizing electrical properties and further supports the scalability of this method for multi-layer device applications.

The Seebeck coefficient for the Sb_2Te_3 thin film, measured in a differential temperature setup, was found to be 195 μV/K at room temperature without annealing. This value aligns well with high-quality Sb_2Te_3 thin films fabricated using alternative advanced methods, indicating the suitability of the PVD process with synthesized nano powders for producing competitive thermoelectric materials.

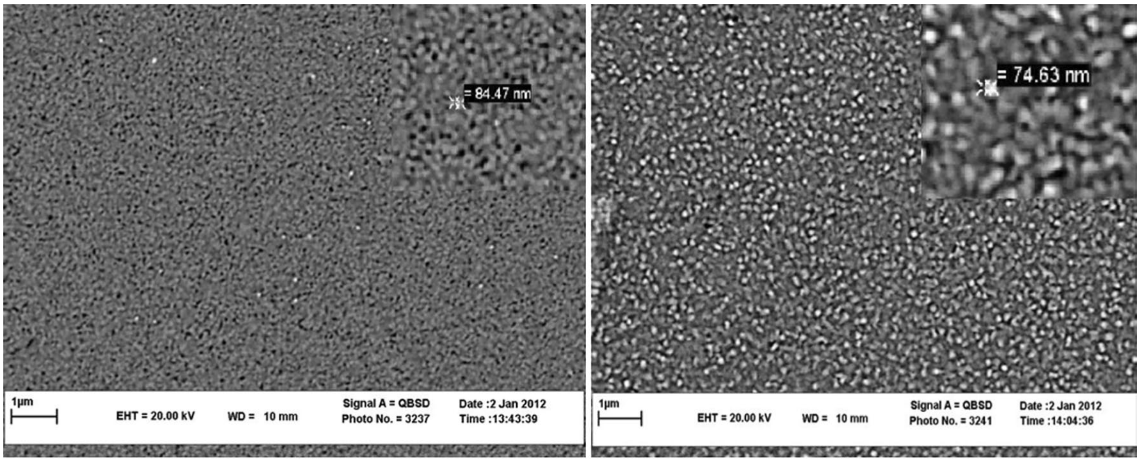

(a) (b)

Fig.2 SEM images of **a** Sb3Te3 thin film, **b** Bi_2Te_3 thin film

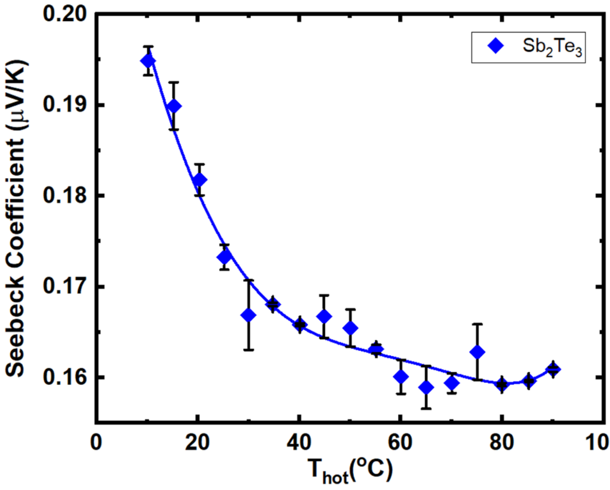

Fig. 3 Seebeck coefficient of Sb_2Te_3 as a function temperature in hot side of the thin film

Upon annealing for one hour at 150°C, the Seebeck coefficient increased to 380 µV/K. This increase is primarily attributed to the annealing-induced enhancement of grain boundary quality, which reduces defect states that typically act as scattering centers for charge carriers. This reduction in carrier scattering leads to improved carrier mobility, allowing higher-energy carriers to contribute more effectively to the thermoelectric voltage. The positive Seebeck coefficient confirms p-type conductivity, where holes dominate charge transport. Temperature-dependent measurements of the Seebeck coefficient for Sb_2Te_3 revealed a sharp decrease from approximately 195 µV/K to around 165 µV/K at $T_{hot} = 50$ °C, as shown in Fig. 3. This initial drop is likely due to increased phonon-electron scattering at elevated temperatures. Phonon-electron interactions become significant as the phonon population increases with temperature, reducing the energy gradient among carriers and consequently lowering the Seebeck coefficient. Beyond $T_{hot} = 50$ °C the Seebeck coefficient stabilizes, forming a plateau up to $T_{hot} = 100$ °C. This stabilization indicates a thermal equilibrium point where the generation of charge carriers due to thermal excitation balances the loss of thermoelectric potential caused by scattering mechanisms. Such behavior is characteristic of materials with well-optimized carrier densities, where competing effects stabilize performance over a certain temperature range.

In contrast, Bi_2Te_3 thin films, known for their n-type conductivity, exhibit a Seebeck coefficient of − 45 µV/K under similar conditions. This negative value reflects electron-dominated transport. After annealing at 150 °C for one hour, the Seebeck coefficient improved to − 170 µV/K, highlighting the role of annealing in optimizing carrier concentration and energy filtering. Energy filtering occurs when grain boundaries selectively scatter lower-energy electrons while allowing higher-energy electrons to contribute to electrical conduction, effectively increasing the Seebeck coefficient.

The temperature dependence of the Seebeck coefficient for Bi_2Te_3 before annealing, shown in Fig. 4, starts at approximately 52 µV/K, peaking at around 56 µV/K at $T_{hot} \approx 40$ °C, before gradually decreasing with increasing temperature. By $T_{hot} \approx 160$ °C, the coefficient drops to approximately 45 µV/K. This

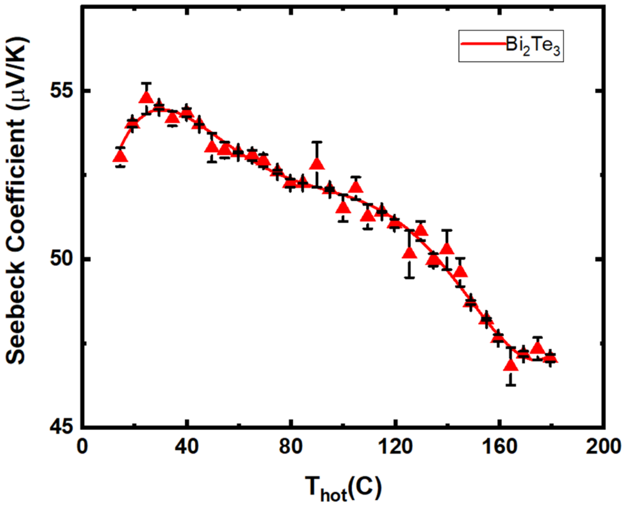

Fig. 4 Seebeck coefficient of Bi_2Te_3 as a function of temperature in hot side of the thin film

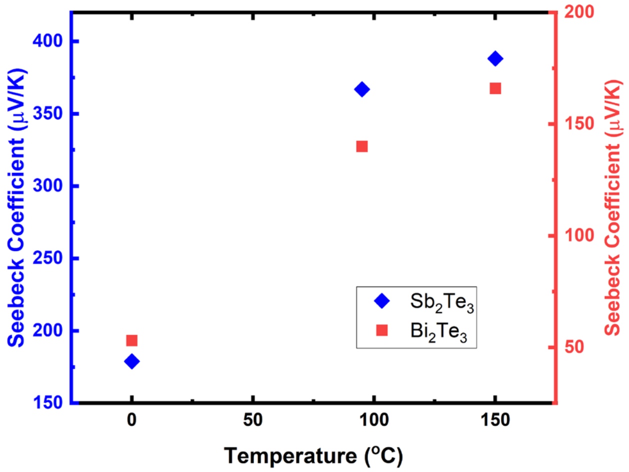

Fig. 5 Seebeck coefficient as a function of annealing temperature

steady decline reflects increased phonon scattering and reduced carrier mobility at higher temperatures. Unlike Sb_2Te_3, Bi_2Te_3 does not exhibit a plateau or recovery phase, suggesting a linear decrease in thermoelectric efficiency with temperature. This behavior indicates Bi_2Te_3's efficiency is better suited for lower temperature environments, where phonon scattering is less significant and carrier transport is more efficient.

The complementary behaviors of Sb_2Te_3 and Bi_2Te_3 highlight their potential in p–n junction thermoelectric devices. When paired, the p-type Sb_2Te_3 and n-type Bi_2Te_3 enable a balanced energy conversion mechanism, as their opposing Seebeck coefficients create a strong thermoelectric voltage gradient. This pairing is particularly advantageous for achieving high efficiency in thermoelectric modules, where the thermal and electrical characteristics of the materials complement each other across a broad temperature range.

Figure 5 compares the Seebeck coefficients of Sb_2Te_3 and Bi_2Te_3 as a function of annealing temperature. For Sb_2Te_3, the Seebeck coefficient begins at approximately 150 μV/K and steadily increases with higher annealing temperatures, reaching around 380 μV/K at the highest annealing temperature. Similarly, Bi_2Te_3 shows a consistent increase from approximately 50 μV/K to about 200 μV/K. This significant improvement in thermoelectric performance is attributed to several interconnected physical mechanisms influenced by the annealing process. Annealing plays a crucial role in reducing defects such as point defects, dislocations, and grain boundary irregularities that hinder charge carrier mobility [31]. These reductions enable carriers to transport more freely, directly enhancing the thermoelectric voltage generated per unit temperature difference [15]. For Sb_2Te_3, the improved transport of high-energy holes enhances the p-type Seebeck coefficient, while in Bi_2Te_3, similar mechanisms optimize electron transport, refining its n-type performance. The annealing process also adjusts carrier concentrations by modifying defect states that contribute to donor or acceptor levels. This rebalancing ensures an optimized interplay between carrier density and mobility, further boosting the Seebeck coefficient in both materials. Additionally, annealing enhances crystallinity by promoting recrystallization, which improves long-range order within the films [32, 33]. This reduces phonon-electron interactions that typically hinder thermoelectric performance, allowing for more efficient energy transport. Another significant factor is the refinement of grain boundaries, which strengthens energy filtering [28]. Well-defined grain boundaries selectively scatter low-energy carriers while permitting high-energy carriers to contribute to electrical conduction, thereby increasing the Seebeck coefficient. Moreover, annealing introduces non-coherent grain boundaries that scatter phonons effectively, reducing lattice thermal conductivity while maintaining electrical transport properties [34]. This combination contributes to a higher thermoelectric performance.

Electrical conductivity, assessed using a two-probe method, yielded a specific resistivity of 43.054 μΩ·m, translating to an electrical conductivity of 28×10^3 S/m at 25 °C for Sb_2Te_3 and 26.355 μΩ·m, 37×10^3 S/m for Bi_2Te_3 respectively. Figure 6 depicts the natural logarithm of resistivity as a function of temperature. For Sb_2Te_3, the resistivity initially decreases slightly with increasing temperature up to approximately 150°C, indicating metallic-like behavior or thermally activated carrier transport. Beyond 200°C, the resistivity increases sharply, likely due to enhanced phonon scattering or structural degradation at higher temperatures. In contrast, Bi_2Te_3 exhibits a consistent decrease in resistivity over the entire temperature range, from approximately 20 °C to 180 °C, suggesting a thermally activated conduction mechanism where the carrier concentration or mobility improves with temperature. The overall behavior of these materials highlights their distinct electrical transport mechanisms, with Sb_2Te_3 showing a transition at elevated temperatures, while Bi_2Te_3 demonstrates a more stable decrease in resistivity, making it potentially more suitable for applications requiring consistent electrical performance over a broader temperature range.

The power factor (*PF*) as shown in Eq. 4 of Sb_2Te_3 and Bi_2Te_3 thin films reached 850 μW/mK^2 and 100 μW/mK^2 at room temperature respectively, a competitive value for thermoelectric applications. Where in this equation α is seebeck coefficient and σ is the conductivity. The power factor of the thin film samples as a function of temperature is shown in Fig. 7. This peak performance at ambient conditions is particularly promising for low-temperature energy conversion applications. The high Seebeck coefficient coupled with moderate conductivity, attributed to the nano-scale grain size and uniform film structure, contributes significantly to this favorable power factor. Comparatively, Bi_2Te_3 films often show a slightly lower power factor due to their n-type characteristics, but they effectively complement the high Seebeck coefficient of enhancing overall thermoelectric efficiency in combined applications.

$$PF = \alpha^2\sigma \tag{4}$$

To better understand the thermoelectric performance of the synthesized Sb_2Te_3 and Bi_2Te_3 materials, their Seebeck coefficient, power factor, and fabrication methods have been compared with those reported in the literature recently. Table 3 provides a summary of these key parameters, highlighting the advantages of the physical vapor deposition (PVD) method used in this work. The comparison underscores the potential of our approach to achieve competitive thermoelectric properties, emphasizing the suitability of nano-engineered materials for advanced thermoelectric applications.

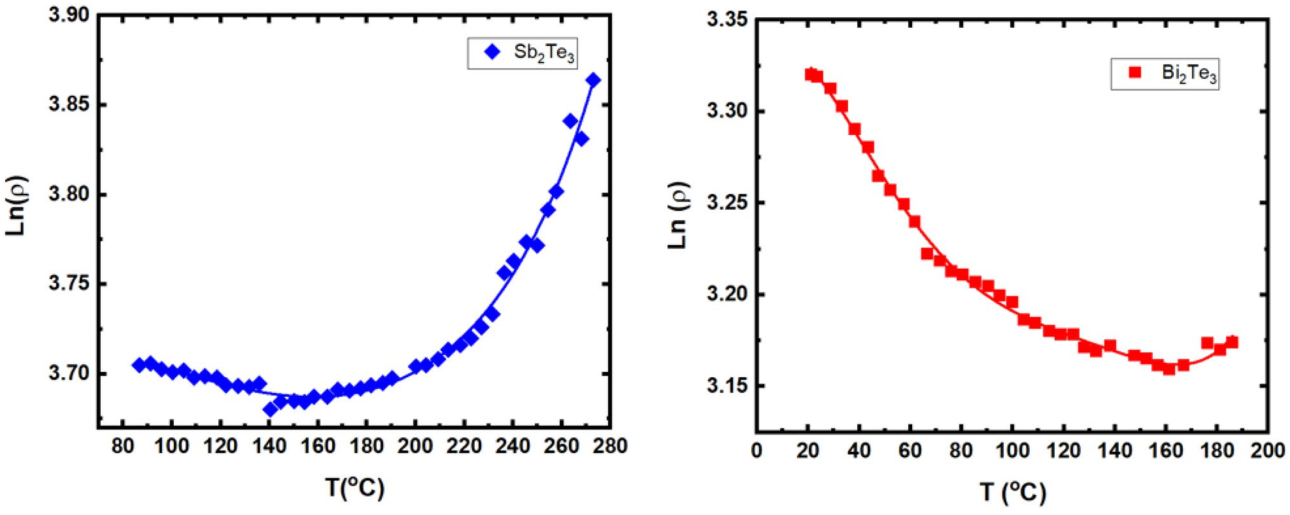

Fig. 6 Natural logarithm of resistivity as a function of temperature for Bi_2Te_3 and Sb_2Te_3 thin films

Fig. 7 Power Factor as a function of temperature for both Sb_2Te_3, and Bi_2Te_3 thin films

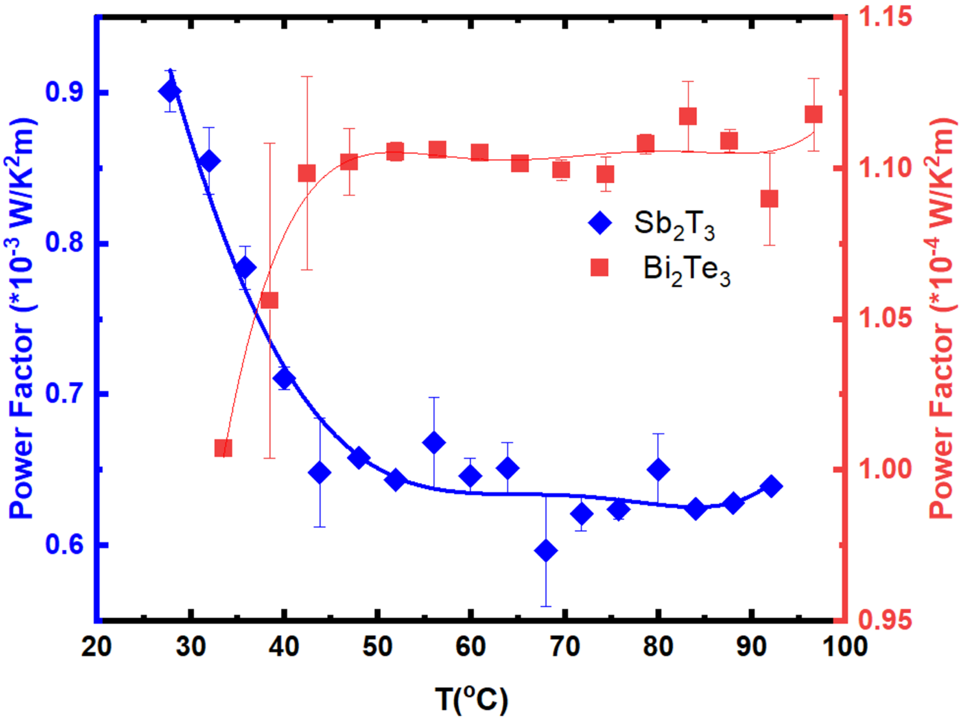

Table 3 Comparison of recent works on Thermoelectric materials

Material	Fabrication method	Seebeck coefficient (μV/K)	References	Year
Sb_2Te_3	PVD	380	–	–
Bi_2Te_3	PVD	170	–	–
Sb_2Te_3	RF magnetron	400	[35]	2022
Ni/ Sb_2Te_3/Ni	RF magnetron	400	[35]	2022
Bi_2Te_3	Electrochemical	20	[9]	2020
$Te_{0.98}As_{0.02}$	Ball mill + Hot press	350	[36]	2020
Au-Sb_2Te_3	Hydrothermal	120	[37]	2025
Sb_2Te_3-MWCNT	–	60	[38]	2023

4 Summary

The manuscript investigates the fabrication and thermoelectric properties of Sb_2Te_3 and Bi_2Te_3 thin films prepared via physical vapor deposition (PVD) using synthesized nano powders. Nano Sb_2Te_3 and Bi_2Te_3 powders were synthesized using a hydrothermal method and characterized to confirm their hexagonal crystal structure and nano-sized grains. These powders were used to deposit thin films with thicknesses of approximately 100 nm. Structural and surface morphology analysis (XRD and SEM) confirmed the phase purity, crystallinity, and uniformity of the films. The thermoelectric properties, including Seebeck coefficient, electrical conductivity, resistivity, and power factor, were thoroughly characterized. The Sb_2Te_3 thin films demonstrated a high Seebeck coefficient of 192 μV/K at room temperature, which improved to 380 μV/K upon annealing. The power factor for Sb_2Te_3 reached 850 $\mu W/K^2 \cdot m$, showcasing its potential for thermoelectric applications. In contrast, Bi_2Te_3 exhibited an n-type behavior with a lower Seebeck coefficient of − 45 μV/K at room temperature, increasing to − 170 μV/K after annealing and the power factor at room temperature measured to be 100 $\mu W/mK^2$. The resistivity trends highlighted distinct electrical transport mechanisms: Sb_2Te_3 displayed metallic-like behavior at lower temperatures, while Bi_2Te_3 showed a consistent decrease in resistivity with temperature, reflecting thermally activated conduction. The complementary thermoelectric characteristics of Sb_2Te_3 and Bi_2Te_3 suggest their potential for use in p-n junctions for high-efficiency thermoelectric devices. The study demonstrates the advantages of using PVD with synthesized nano powders to achieve high-performance thermoelectric thin films, emphasizing the role of nano structuring, annealing, and precise deposition techniques.

Author contribution

M.R. Roknabad: Analysis, interpretation of data, supervision, revising the content, confirming the result. M. Mollaee: Doing the experiment, analyzing the result, draft the manuscript. S. Garazhian: Doing the experiment, data analysis.

Funding

The authors declare that no funds, grants, or other support were received during the preparation of this manuscript.

Research data policy and data availability

The authors declare that the data supporting the findings of this study are available within the paper.

Declarations

Competing interest The authors declare that they have no known competing financial interests or personal relationships that could have appeared to influence the work reported in this paper.

References

1. Q. Zhang, Y. Sun, W. Xu, D. Zhu, Adv. Mater. **26**, 6829 (2014)
2. S. Twaha, J. Zhu, Y. Yan, B. Li, Renew. Sustain. Energy Rev. **65**, 698 (2016)
3. M. Hamid Elsheikh, D.A. Shnawah, M.F.M. Sabri, S.B.M. Said, M. Haji Hassan, M.B. Ali Bashir, M. Mohamad, Renew. Sustain. Energy Rev. **30**, 337 (2014)
4. F.M. Yildirim, V. Ugraskan, O. Yazici, J. Mater. Sci. Mater. Electron. **34**, 1 (2023)
5. H.H. Radamson, A. Hallén, I. Sychugov, A. Azarov, *Analytical Methods and Instruments for Micro- and Nanomaterials* (Springer, Cham, 2023)
6. J.E. Hong, S.K. Lee, S.G. Yoon, J. Alloys Compd. **583**, 111 (2014)
7. J.M. Lin, Y.C. Chen, C.F. Yang, W. Chen, J. Nanomater. Nanomater. **2015**, 135130 (2015)
8. P. Wanarattikan, P. Jitthammapirom, R. Sakdanuphab, A. Sakulkalavek, Adv. Mater. Sci. Eng. **2019**, 6954918 (2019)
9. J. Recatala-Gomez, P. Kumar, A. Suwardi, A. Abutaha, I. Nandhakumar, K. Hippalgaonkar, Sci. Rep. **10**, 1 (2020)
10. N. Peranio, O. Eibl, J. Nurnus, J. Appl. Phys. **100** (2006)
11. H. Osterhage, J. Gooth, B. Hamdou, P. Gwozdz, R. Zierold, K. Nielsch, Appl. Phys. Lett. **105**, (2014)
12 J.F. Li, W.S. Liu, L.D. Zhao, M. Zhou, NPG Asia Mater. **2**, 152 (2010)
13. J.R. Szczech, J.M. Higgins, S. Jin, J. Mater. Chem. **21**, 4037 (2011)
14. J.J. Kuo, M. Wood, T.J. Slade, M.G. Kanatzidis, G.J. Snyder, Energy Environ. Sci. **13**, 1250 (2020)
15. S. Kianwimol, R. Sakdanuphab, N. Chanlek, A. Harnwunggmoung, A. Sakulkalavek, Surf. Coat. Technol. **393**, 125808 (2020)
16. Z. Soleimani, S. Zoras, B. Ceranic, S. Shahzad, Y. Cui, Sustain. Energy Technol. Assess. **37**, 100604 (2020)
17. W. Liu, L. Endicott, V.A. Stoica, H. Chi, R. Clarke, C. Uher, J. Cryst. GrowthCryst. Growth **410**, 23 (2015)
18. H. Shankar, N. S, P. Veluswamy, (n.d.)
19. I.T. Witting, T.C. Chasapis, F. Ricci, M. Peters, N.A. Heinz, G. Hautier, G.J. Snyder, Adv. Electron. Mater. **5**, 1800904 (2019)
20. J.H. Kim, J.Y. Choi, J.M. Bae, M.Y. Kim, T.S. Oh, Mater. Trans. **54**, 618 (2013)
21. K.D.A. Kumar, D.K. Meena, R.S.C. Bose, R. Meena, P. Murahari, P. Mele, K. Ramesh, J. Alloys Compd. **865**, 158621 (2021)
22. F. Moshtaghi, M. Yousefpour, A. Habibolahzadeh, Mater. Sci. Eng. B **296** (2023)
23. S. Thaowonkaew, M. Insawang, A. Vora-ud, M. Horprathum, P. Muthitamongkol, S. Maensiri, M. Kumar, T.B. Phan, T. Seetawan, Vacuum **211**, 111920 (2023)
24. K.W. Cheng, C.H. Kung, J.Y. Huang, C.H. Ku, Q.M. Huang, V.K. Ranganayakulu, Y.Y. Chen, S.J. Chiu, Y.G. Lin, C.M. Wang, A.T. Wu, Mater. Chem. Phys. **318**, 1 (2024)

25. M. Noroozi, G. Jayakumar, K. Zahmatkesh, J. Lu, L. Hultman, M. Mensi, S. Marcinkevicius, B. Hamawandi, M.Y. Tafti, A.B. Ergül, Z. Ikonic, M.S. Toprak, H.H. Radamson, ECS J. Solid State Sci. Technol. **6**, Q114 (2017)
26. Y. Li, G. Wang, M. Akbari-Saatlu, M. Procek, H.H. Radamson, Front. Mater. **8**, 611078 (2021)
27. H.L. Ni, X.B. Zhao, T.J. Zhu, X.H. Ji, J.P. Tu, J. Alloys Compd. **397**, 317 (2005)
28 G.J. Snyder, E.S. Toberer, Nat. Mater. **7**, 105 (2008)
29. H. Li, X. Su, X. Tang, Q. Zhang, C. Uher, G.J. Snyder, U. Aydemir, J. Mater. **3**, 273 (2017)
30. Z.G. Chen, G. Hana, L. Yanga, L. Cheng, J. Zou, Prog. Nat. Sci. Mater. Int. **22**, 535 (2012)
31. M. Zebarjadi, K. Esfarjani, M.S. Dresselhaus, Z.F. Ren, G. Chen, Energy Environ. Sci. **5**, 5147 (2012)
32. F.J. Humphreys, M. Hatherly, *Recrystallization and Related Annealing Phenomena* (Elsevier, Amsterdam, 2012)
33. J. Yang, H. Hu, Y. Miao, B. Wang, W. Wang, H. Su, Y. Ma, J. Phys. D Appl. Phys. **53**, 265105 (2020)
34. M. Schrade, K. Berland, S.N.H. Eliassen, M.N. Guzik, C. Echevarria-Bonet, M.H. Sørby, P. Jenuš, B.C. Hauback, R. Tofan, A.E. Gunnæs, C. Persson, O.M. Løvvik, T.G. Finstad, Sci. Rep. **7**, 1 (2017)
35. Z. Sun, K. Cheng, S. Lin, V. K. Ranganayakulu, Y. Chen, S. Chiu, T. Lee, A. T. Wu (2022)
36. Y. Wu, F. Liu, Q. Zhang, T. Zhu, K. Xia, X. Zhao, J. Mater. Chem. A **8**, 8455 (2020)
37. N. Komal, M. A. Mansoor, M. Sohail, G. A. Chotana, M. Anis-ur-Rehman, M. Mazhar, Phys. B Condens. Matter (2025)
38. J. Andzane, E. Spalva, J. Katkevics, L. Bugovecka, A. Kons, K. Buks, D. Erts, A.C.S. Appl, Energy Mater. **6**, 10807 (2023)